



OPEN

Porous mesocarbon microbeads with graphitic shells: constructing a high-rate, high-capacity cathode for hybrid supercapacitor

Yu Lei¹, Zheng-Hong Huang¹, Ying Yang², Wanci Shen¹, Yongping Zheng¹, Hongyu Sun¹ & Feiyu Kang¹¹Key Laboratory of Advanced Materials (MOE), School of Materials Science and Engineering, Tsinghua University, Beijing 100084, China, ²Department of Electrical Engineering, Tsinghua University, Beijing 100084, China.

Li₄Ti₅O₁₂/activated carbon hybrid supercapacitor can combine the advantages of both lithium-ion battery and supercapacitor, which may meet the requirements for developing high-performance hybrid electric vehicles. Here we proposed a novel “core-shell” porous graphitic carbon (PGC) to replace conventional activated carbon for achieving excellent cell performance. In this PGC structure made from mesocarbon microbead (MCMB), the inner core is composed of porous amorphous carbon, while the outer shell is graphitic carbon. The abundant porosity and the high surface area not only offer sufficient reaction sites to store electrical charge physically, but also can accelerate the liquid electrolyte to penetrate the electrode and the ions to reach the reacting sites. Meanwhile, the outer graphitic shells of the porous carbon microbeads contribute to a conductive network which will remarkably facilitate the electron transportation, and thus can be used to construct a high-rate, high-capacity cathode for hybrid supercapacitor, especially at high current densities.

The development of hybrid electric vehicles (HEVs) has urged worldwide researchers to develop fast charging and high energy density electrochemical energy storage cells which are typically needed upon driving to accelerate or slow the car¹. Up to date, one of the most promising electrochemical cells to achieve fast charging and discharging is the electric double layer capacitor (EDLC)²⁻⁵, which includes aqueous and nonaqueous systems. EDLCs are energy storage devices that allow exceptionally fast charge/discharge, robustness and capacitance exceeding that of electrolytic capacitors^{6,7}. The nonaqueous EDLC displays a preferable performance due to a wider working voltage window, resulting in higher energy densities in comparison with the aqueous EDLC. However, compared with Li-ion battery, the nonaqueous EDLC still has a limited energy density, which is restricted to deliver power in several seconds required by HEV applications⁸. In order to enhance the energy density, tremendous efforts have been undertaken to improve the performance of EDLC, in particular by constructing pseudocapacitive electrodes^{4,5,9-14}. The addition of faradaic process which occurs in parallel with a double-layer capacitance can effectively improve the electrochemical performance. The surfaces of electrodes are the main reaction sites for pseudocapacitive process, which avoid the stresses from bulk intercalation reactions. Without the electrochemical breakdown from bulk intercalation materials, the hybridization of the double-layer and pseudocapacitive electrodes exhibits superb reversibility at high current densities, which results in both high energy density and fast charge capability.

Recently, the hybridization of EDLC and lithium-ion battery is attracting more and more attention¹⁵. Using the activated carbon electrode to replace one of lithium-ion battery electrodes¹⁶ was originally introduced as “asymmetric hybrid nonaqueous energy storage cell (AHEC)” by Glenn G. Amatucci *et al.*¹⁷. Lithium titanate (Li₄Ti₅O₁₂, LTO) has been recognized as an excellent anode material for high-rate lithium batteries, since its “zero strain” lithium insertion properties¹⁸. By using Li₄Ti₅O₁₂ as anode material, the AHEC exhibits long cyclic stability and high rate performance¹⁷. However, the low electronic conductivity (<10⁻⁹ S cm⁻¹) of Li₄Ti₅O₁₂ restricts the further improvement. Several approaches have been carried out to improve its conductivity, for instance, by combining it with conductive carbon materials. Recently, our group found that the charge-transfer resistance can be reduced sharply by coating a thin carbon layer with thickness ~1 nm¹⁹. Besides, a nanostructured Li₄Ti₅O₁₂ was employed as the lithium-ion battery electrode^{17,20}. The authors demonstrated that

SUBJECT AREAS:

ELECTROCHEMISTRY
SYNTHESIS AND PROCESSING
NANOPARTICLES
BATTERIESReceived
27 March 2013Accepted
31 July 2013Published
21 August 2013Correspondence and
requests for materials
should be addressed to
Z.-H.H. (zhhuang@
tsinghua.edu.cn) or
F.Y.K. (fykang@mail.
tsinghua.edu.cn)



the 3 V hybrid supercapacitor was able to deliver 11 Wh kg⁻¹ energy density and up to 4 kW kg⁻¹ power density²¹. However, poor electronic conductivity (<10⁻¹³ S cm⁻¹)²² and sluggish Li⁺ diffusion (<10⁻⁶ cm² s⁻¹)²³ are the biggest obstacles for as-fabricated Li₄Ti₅O₁₂ electrodes. In order to balance the slow faradic process and double-layer capacitance, the poor power performance of Li₄Ti₅O₁₂ should be improved by combining Li₄Ti₅O₁₂ with some electrically conductive materials or nanocrystallization. In 2009, Naoi *et al.* synthesized a nano-structured nc-LTO/CNF composite to replace the common nano-structured Li₄Ti₅O₁₂⁸. This replacement of cathode material led to the increase in both power density and energy density. The hybrid supercapacitor with the weight ratio of LTO/CNF (carbon nanofiber) = 70/30 exhibited an energy density as high as 40 Wh L⁻¹ and power density up to 8 kW L⁻¹. A hyper-networked LTO/carbon hybrid nanofiber sheets were also synthesized to employ as the anode in LTO/activated carbon hybrid supercapacitor²⁴. The nanofiber sheets were synthesized by electrospinning and vapor polymerization techniques. The electrospun nanofibers were beneficial for the formation of 3-D conductive network, which contributed to the improvement of electronic conductivity. This hybrid supercapacitor exhibited energy densities ranged from 91 to 17 Wh kg⁻¹ and power densities ranged from 50 to 4000 W kg⁻¹. Compared to Li₄Ti₅O₁₂, Ti₂C has better electronic conductivity as the anode material of the hybrid supercapacitor which exhibits a maximum energy density of 30 Wh kg⁻¹ at 930 W kg⁻¹ of active materials for 1000 cycles²⁵. Besides, conducting polymers, such as polyaniline (PANI) and polypyrrole (PPy), are employed to synthesize high rate electrodes for hybrid supercapacitor^{26,27}.

Though many efforts have been made to increase the power capacity of anode Li₄Ti₅O₁₂, little work is focused on the replacement of activated carbon for the cathode material of LTO/activated carbon hybrid supercapacitor. Until recently, Ruoff *et al.* synthesized a chemically activated graphene ('activated microwave expanded graphite oxide', a-MEGO)^{28,29}, which can be used as a cathode material to replace commercial activated carbon in LTO/activated carbon hybrid supercapacitor³⁰. The a-MEGO possessed not only a high surface area of 3100 m² g⁻¹, but also a high conductivity contributed by graphene structure. This multi-structure has yielded an excellent performance with common Li₄Ti₅O₁₂ anode. The hybrid supercapacitor delivered an energy density of 40.8 Wh kg⁻¹ with an operating voltage of 2.4 V. In this sense, higher power capability contributed by the enhancement of conductivity can allow us to replace the activated carbon cathode material in LTO/activated carbon hybrid supercapacitor with a porous graphitic carbon (PGC). In present work, we proposed a novel PGC structure with a graphitic "shell" and an amorphous carbon core. The designed graphitic shell contributes to continuous conductive network. In the meanwhile, substantial energy can be stored in the porous core which may serve as an excellent cathode material for hybrid supercapacitor.

Results

The synthetic procedure of PGC with a unique core-shell structure from mesocarbon microbeads (MCMB) is schematically illustrated in Figure 1. As presented in Figure S1 (a) and (b), activation with NaOH transformed MCMB into porous carbon materials with dominant micropores. Such materials possessed a relatively high specific area of 929 m² g⁻¹ measured by a volumetric adsorption system. Moreover, catalytic graphitization with FeCl₃·H₂O converted certain parts of the porous MCMB into graphitic carbons, which was demonstrated by the sharp peak around 2θ = 26.4° of the XRD pattern in Figure S1(c).

The morphology of the as-prepared PGC was characterized by scanning electron microscopy (SEM), high resolution transmission electron microscopy (HRTEM), and the Raman spectrometer. As shown in Figure 2(a), the PGC particles with diameters ranging from 10 to 20 μm remained spherical shape after the calcination. Figure 2(b) is the HRTEM image of the PGC particle which was ground by agate mortar in prior to ultrasonic dispersion in ethanol. Both graphene ribbons with 10 to 30 layers thick and disordered amorphous carbon can be seen in the Figure 2 (b), which suggests that the PGC processes a multi-structure with both graphitic and amorphous structures.

In order to observe the cross-section morphology of as-synthesized PGC, it was embedded into resin and sliced up for further HRTEM observation. The corresponding SEM image is shown in Figure 2(c). As shown in the HRTEM image of Figure 2(d), well-stacked sheets along the in-plane direction as well as the random orientations are observed for the microbead's surface layer, while the interior structure is still mainly amorphous carbon. Additionally, the micro-Raman spectroscopy of the outside surface of the microbead implies higher graphitization degree than that of the interior part. All these results indicate a graphitic shell structure of the PGC particles as illustrated in Figure 1. When PGC was fabricated into cathode, the graphitic shells of PGC will form conductive network if their concentration can reach the threshold value. This will be beneficial for the improvement of power capability. Meanwhile, the porous core structure with high porosities offers sufficient sites for the charge storage process, which guarantees a significant capacity. Such a porous microbead with a graphitic shell is expected to result in excellent electrochemistry performances when they are used to replace the commercial activated carbon as the cathode material in hybrid supercapacitor.

The cathode performances of the synthesized PGC and commercial available activated carbon YP-17D were evaluated in a half-cell with the potential window from 2 to 4.5 V (vs. Li/Li⁺). Figure 3(a) shows the charge-discharge curves for two cells at current density of 70 mA g⁻¹ and IR drops (the voltage decrease at the switching point) which can reflect the conductivity of electrode material. The IR drop at the beginning of constant current discharge of PGC is about

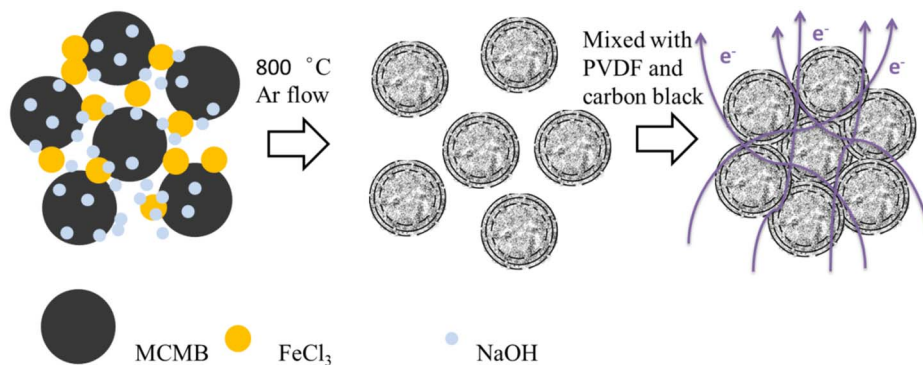


Figure 1 | Schematic illustration of the formation of PGC and the PGC electrode.

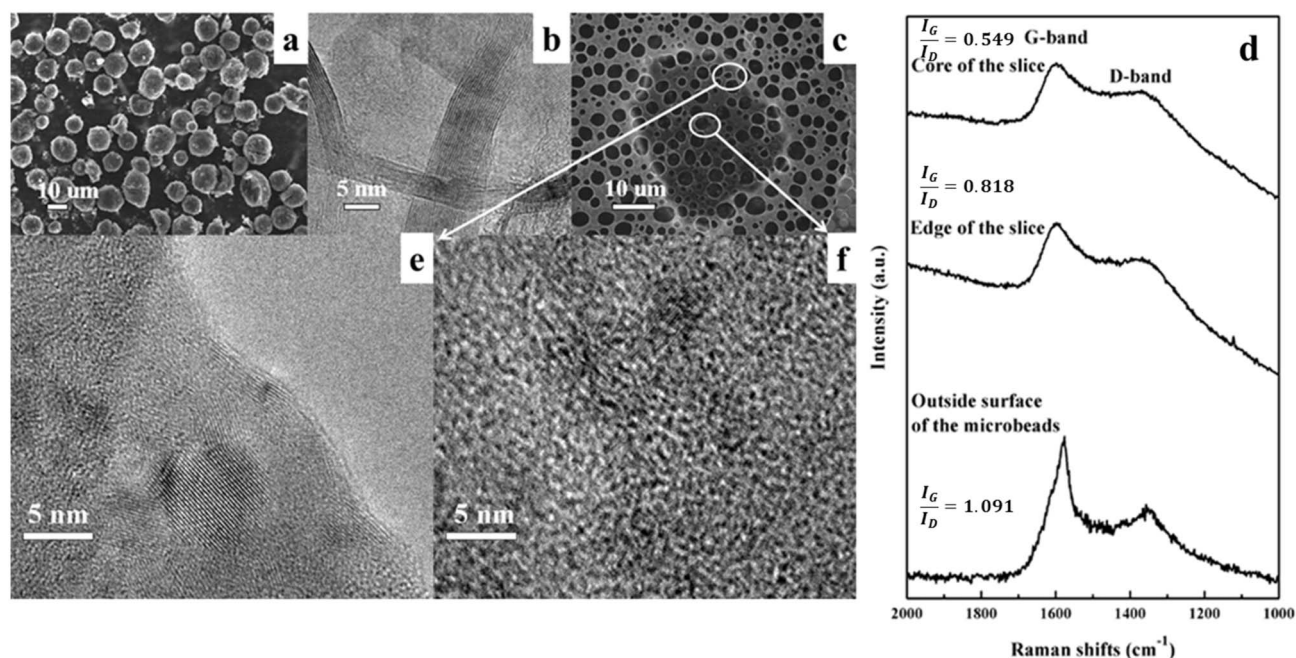


Figure 2 | Morphological and structural analysis of PGC. (a) SEM image of MCMB-based PGC; (b) HRTEM image of PGC powders; (c) SEM image of the PGC slice on a Cu TEM mesh; (d) HRTEM image of the edge of the slice shown in Fig. 2(c); (e) HRTEM image of the core of the slice shown in Fig. 2(c); (f) Raman spectra of the outside surface of PGC particles and the core or edge of the slice.

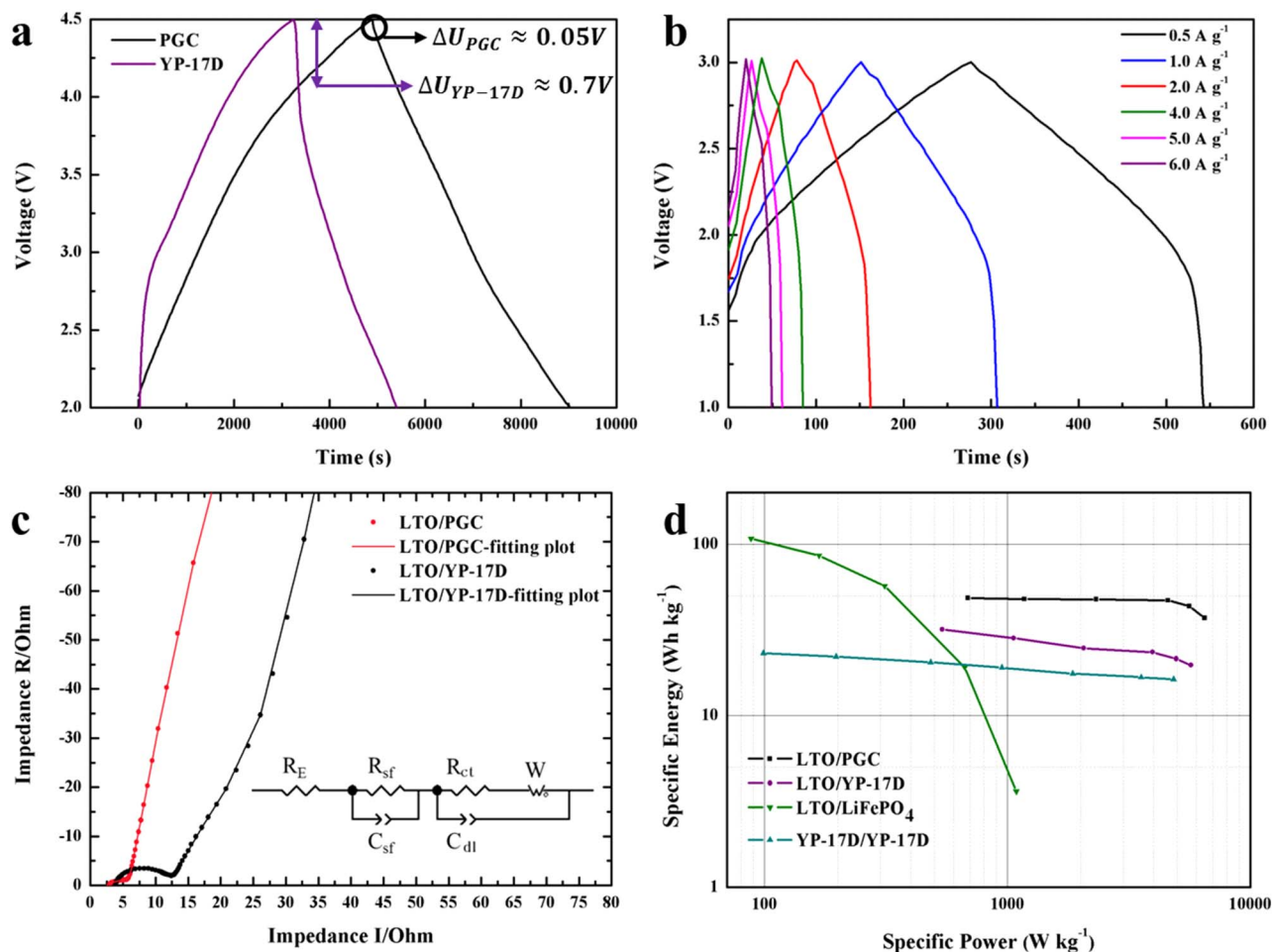


Figure 3 | (a) the charge-discharge curves of half cells: the PGC and YP-17D electrodes. (b) Charge/discharge curves for LTO/PGC hybrid supercapacitor. (c) AC impedance plots of LTO/PGC and LTO/YP-17D hybrid supercapacitors. The equivalent circuit is given in the inset. (d) Ragone plots of the LTO/PGC and LTO/YP-17D hybrid supercapacitors obtained from the discharge curves measured at different constant current densities.



0.05 V which is about 14 times lower than that of YP-17D. Therefore, the half-cell fabricated with the PGC shows a much lower equivalent series resistance than those fabricated with YP-17D, which indicates that PGC is a preferable cathode owing to its graphitic shell.

Figure 3(b) shows the charge-discharge curves for a full hybrid supercapacitor assembled with 1.5 : 1 weight ratio of PGC cathode to $\text{Li}_4\text{Ti}_5\text{O}_{12}$ anode. From the discharge part of the curves, the energy densities are 48.7, 47.9, 47.6, 47.1, 43.4, and 37.2 Wh kg^{-1} for current densities of 0.5, 1, 2, 4, 5, and 6 A g^{-1} , respectively. The energy densities were calculated with the total mass of the active materials for both two electrodes. The voltage profiles at various current densities share a certain characteristic. That is the early discharge state of LTO/PGC hybrid supercapacitor reveals a gradually sloping profile between 2 and 3 V compared with sharply sloped profile between 1 and 2 V. The significant change in slope indicates the differences in energy storage mechanisms. The EDLC of the carbon species in the LTO/PGC contributes to the linear profile. Simultaneous with the PF_6^- anion double layer forming on the surface of two electrodes, a Li^+ ion lithiation/delithiation reaction occurs at the anode electrode. The hybridization electrode reactions lead to the gradually sloping profile ranged from 2 to 3 V^{17,24}. These results suggest that hybridization of PGC with $\text{Li}_4\text{Ti}_5\text{O}_{12}$ can enhance the energy density compared with an EDLC because of the additional intercalation reaction from $\text{Li}_4\text{Ti}_5\text{O}_{12}$.

Electrochemical impedance spectroscopies (EIS) of the LTO/PGC and LTO/YP-17D hybrid supercapacitors are plotted in Figure 3(c). For two cells, the EIS are composed of two partially overlapped semicircles at high frequency and a straight slopping line at low frequency. An equivalent circuits, as shown in the inset figure, can be employed to fit the EIS patterns³¹. Here R_E denotes the bulk resistance of the cell including resistance of the electrolyte, separator and electrodes. R_{sf} and C_{sf} are resistance and capacitance of the surface film on two electrodes, which correspond to the overlapped semicircle at high frequencies. R_{ct} and C_{dl} are charge transfer resistance and the double-layer capacitance, which are related to the semicircle at medium frequencies. The straight slopping line at low frequencies is related to the Warburg impedance (W) related to the diffusion of lithium ions on the electrode-electrolyte interfaces^{31,32}. The fitting results including R_{sf} , R_{ct} , and R_E are summarized in Table 1, and the surface film resistances (R_{sf}) are similar for two hybrid supercapacitors. However the bulk resistance (R_E) and charge transfer resistance (R_{ct}) for LTO/PGC hybrid supercapacitor are lower than those of LTO/YP-17D hybrid supercapacitor, especially charge transfer resistance. The replacement of commercial activated carbon (YP-17D) by PGC dramatically reduces the R_{ct} from 5.3 ohm to only 0.05 ohm. The highly conductive PGC remarkably enhances the conductivity of the hybrid supercapacitors, which couples well with the ESR analysis above. Since the PGC particle possesses a porous structure with a graphitic shell, this multi-structure is beneficial to enhance the electronic conduction, which reduces the electronic resistance effectively as shown in Table 1^{33,34}. All these results indicate a considerable performance of LTO/PGC hybrid supercapacitor by the aid of the multi-structure of PGC, which leads to improved high-rate capabilities of the hybrid supercapacitor.

To examine the effectiveness of PGC with a unique core-shell structure in improving the rate capabilities of $\text{Li}_4\text{Ti}_5\text{O}_{12}$ based hybrid supercapacitor, we investigated the energy density and power density

at different charge/discharge rates which are 0.5 A g^{-1} , 1 A g^{-1} , 2 A g^{-1} , 4 A g^{-1} , 5 A g^{-1} and 6 A g^{-1} . As shown in Figure 3(d), the gravimetric energy densities and power densities on the basis of the total mass of the active materials for both two electrodes are plotted, which called Ragone plot³⁵. For comparison, a LTO/LiFePO₄ lithium-ion battery and a conventional EDLC (AC|LiPF₆-EC-DMC|AC) were also assembled and tested under various current densities. The LTO/LiFePO₄ lithium-ion battery has the highest energy density under low power density; however the reduction of energy density as the increasing of the power density also remains the highest. At a relatively low power density (below 1 kW kg^{-1}), the LTO/PGC hybrid supercapacitor shows energy density nearly 50 Wh kg^{-1} , which is almost 1.5 times higher than that of LTO/YP-17D hybrid supercapacitor and 2 times higher than that of the EDLC. Moreover, the LTO/PGC hybrid supercapacitor exhibits a maximum energy density of 55 Wh kg^{-1} as shown in Figure 4(b). As the current density increases to 4 A g^{-1} , the energy density of LTO/PGC hybrid supercapacitor is barely changed and remains 96.8% of the energy density at 0.5 A g^{-1} . Simultaneous with the 96.8% retention of the energy density, the power density increases 6.7 times, from 686.9 W kg^{-1} at 0.5 A g^{-1} to 4572.9 W kg^{-1} at 4 A g^{-1} . Even at a high power density of about 6500 W kg^{-1} , the energy density still remains 37 Wh kg^{-1} which is almost double that of the LTO/YP-17D hybrid supercapacitor and 2.3 times higher than that of the EDLC. These results reveal that the LTO/PGC hybrid supercapacitor can provide higher energy as compared with the LTO/YP-17D hybrid supercapacitor and EDLC at various power densities, and exhibits better power performance than that of the LTO/LiFePO₄ lithium-ion battery. Accordingly, this specific system is anticipated as an energy device optimized for both high energy and high power applications.

Since the densities vary greatly among activated carbon and LiFePO₄ (the data supplied in the supplementary information), the volumetric Ragone plots were also employed to investigate the differences between LTO/PGC, LTO/YP-17D and LTO/LiFePO₄, as shown in Figure S2. A similar trend with the gravimetric Ragone plots was found based on Figure 3(d). The LTO/PGC delivers 44.5 Wh L^{-1} at 628 W L^{-1} , and 34 Wh L^{-1} at 6000 W L^{-1} . Rather than gravimetric, volumetric energy and power densities reflect the significant performances of LTO/PGC hybrid supercapacitor³⁶.

Discussion

Comparing the rate capabilities of LTO/YP-17D and LTO/PGC hybrid supercapacitors, shown in Figure 3, it indicates that the graphitic shell of PGC stabilizes the electrochemical reactions at high current densities. Since the graphite crystallites are formed at the surface of the porous particles, the faradaic reactions of PGC electrodes occur at the surface. Moreover, since the intercalation reaction sites almost exist at the surface, no bulk intercalation reactions occur, which reduces the risk of electrochemical breakdown resulted in intercalation stresses.

Besides the surface intercalation reactions of the graphitic shell, its existence also leads to the increase of conductivity. To further illustrate the significant performance of PGC, we conducted a comparison analysis to reveal the importance of the graphitic shell on PGC. As illustrated in Figure 4(a), the cathode of LTO/PGC hybrid supercapacitor consists of 80% PGC, 10%PVDF and 10% carbon black (Super P, short for SP). Due to the graphitic shell, the contacts between PGC particles in the electrode contribute to a fine conductive network. However there are still interspaces between particles, which attribute to the weak links among the network. Therefore, the 10% carbon black fills the interspaces and reinforces the weak links, which guarantees the stability at high current density. AMSP is the electrode with 80% activated MCMB, which is denoted as AM, 10%PVDF and 10% carbon black. The difference between M80 and AMSP is the absence of graphitic shell for AMSP. Carbon black

Table 1 | Summaries of the EIS fitting results

Hybrid Supercapacitor	R_E (Ω)	R_{sf} (Ω)	R_{ct} (Ω)
LTO/PGC	2.7	1.5	0.05
LTO/YP-17D	4.0	1.2	5.3
LTO/AMSP	3.2	0.6	1.2
LTO/AMCNT	3.3	0.9	0.5

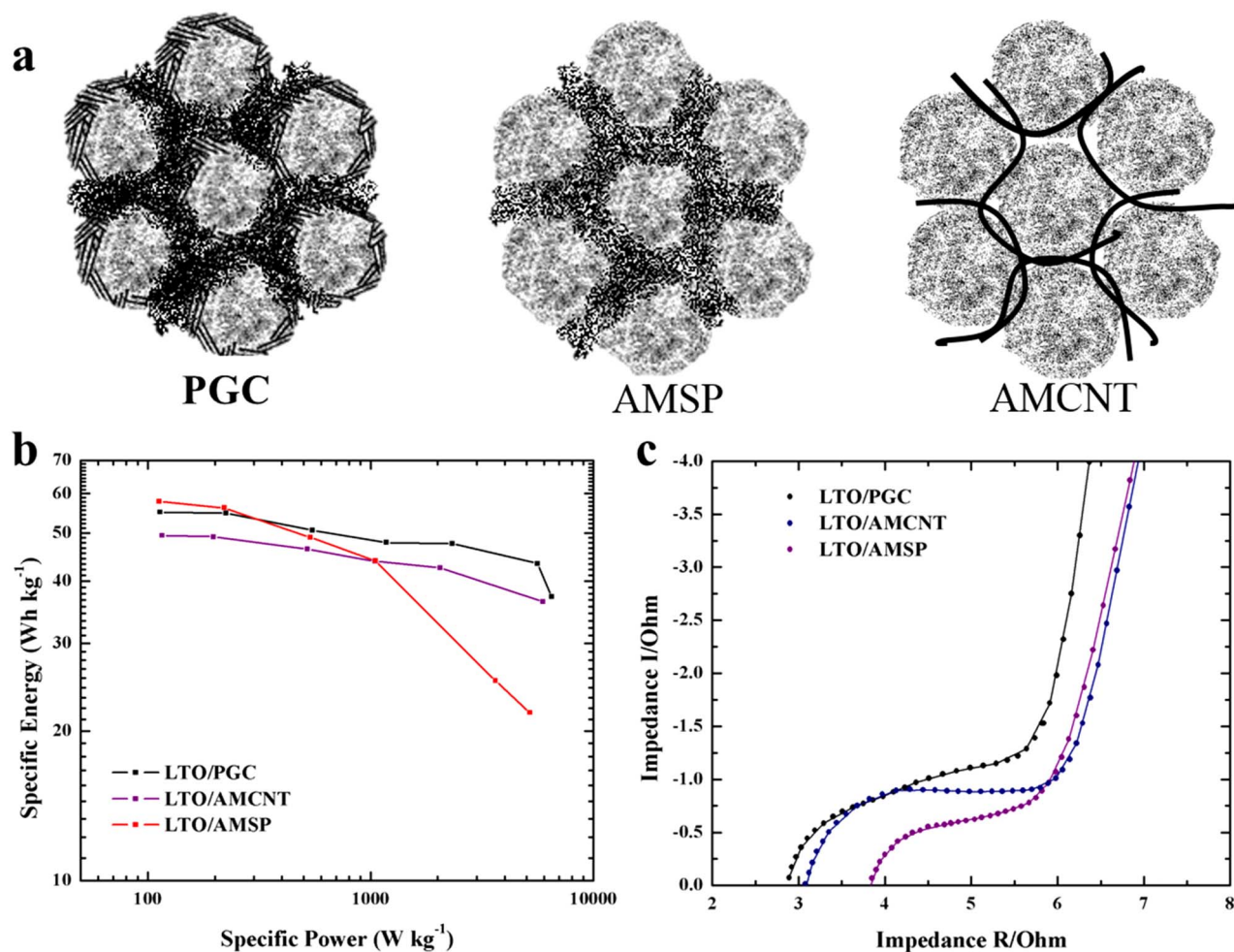


Figure 4 | Schematic illustrations and electrochemical performance comparison among three different cathodes. (a) Schematic illustrations of cathode of PGC, AMCNT and AMSP; (b) Rate performance of LTO/PGC, LTO/AMCNT and LTO/AMSP hybrid supercapacitors; (c) AC impedance plots of LTO/PGC, LTO/AMCNT and LTO/AMSP hybrid supercapacitors.

serves as the only contribution to conductivity. By replacing the carbon black to carbon nanotube (CNT), AMSP turns into AMCNT. Since CNT is a flexible one-dimensional conductor with the rolled graphene structure, the addition of CNT offers a fine conductive network among the AM particles. Figure 4 (b) is the comparison of rate performances among LTO/PGC, LTO/AMSP and LTO/AMCNT. All the hybrid supercapacitors were charged and discharged at 100 mA g⁻¹, 200 mA g⁻¹, 500 mA g⁻¹, 1 A g⁻¹, 2 A g⁻¹, 4 A g⁻¹ and 6 A g⁻¹. At relatively high current densities, LTO/PGC displays higher and more stable performances compared with the others. We also performed EIS tests among the three hybrid devices, as shown in Figure 4(c). The charge transfer resistance (R_{ct}) of LTO/PGC is the smallest, which is listed in Table 1. Since the R_{ct} reflects both electronic and ionic conductivity. Thus the LTO/PGC with both high electronic and ionic conductivity exhibits an excellent rate performance, which is confirmed in Figure 4b. For the LTO/AMSP hybrid supercapacitor, the conductive network constituted by carbon black may be discrete, which results in the ion diffusion blockage and poor conductivity. In addition, for the LTO/AMCNT hybrid supercapacitor, even though the conductivity of CNT is significant high, the physical contact between CNT and amorphous MCMB spheres weakens the conductive network due to its instability. In comparison, the conductivity contributed by graphitic shells and carbon black filler performs more stable and superior than conductivity contributed by either carbon black or other conductive network such as CNT network.

In summary, we synthesized porous graphitic carbons characterized by a unique structure of graphitic shell and an amorphous core from MCMBs. TEM and micro-Raman analyses confirmed the graphitic shell at the activated MCMB particles. When applied as cathode in hybrid supercapacitor, the unique core-shell structure particles delivered high energy density of 55 Wh kg⁻¹ and high power density of 6474.7 W kg⁻¹, which is almost twice higher than that of hybrid supercapacitor with a commercial activated carbon (YP-17D) cathode. It exemplifies that the great potential of PGC with a unique core-shell structure to be used in hybrid supercapacitor, possessing high energy density and high power density.

Methods

Synthesis of the porous graphitic carbon. The porous graphitic carbon was synthesized from mesocarbon microbeads (MCMB) by one-step method^{37,38}. The raw material MCMB was mixed with chemical activation reagent NaOH and graphitization catalyst FeCl₃·H₂O. The ratio of NaOH to MCMB was 4:1 (wt.), and FeCl₃·H₂O was 10 wt.% of MCMB. Then the mixture was calcinated at 800 °C for an hour in an Argon flow. After the sample was cooling to the room temperature, acid and deionized water were employed to wash the sample until the pH value reached to 7. Finally the MCMB-based PGC can be obtained after drying at 100 °C overnight. Activation with NaOH transformed MCMB into a carbon material consisting of micropores ranged from 1 nm to 4 nm and a relatively high specific area of 929 m²·g⁻¹ as measured by a volumetric adsorption system. Moreover catalytic graphitization of FeCl₃·H₂O turned the porous MCMB into a “core-shell” structure with the outer partially graphitized carbon layers.

Materials characterization. The morphology was examined with a LEO-1530 scanning electron microscope. Raman spectrometer (RM2000) and high-resolution



transmission electron microscope (HRTEM) were employed to characterize the surface graphitization of the carbon microbeads.

Electrochemical measurements. For cathode material of battery tests, the activated carbon (PGC or commercial available activated carbon YP-17D) or LiFePO_4 was mixed with 10% binder (PVDF), 10% carbon black (Super P) and NMP. And the slurry was coated onto an aluminum foil. For anode material, $\text{Li}_4\text{Ti}_5\text{O}_{12}$ powder was mixed with PVDF, carbon black and NMP at the same ratios. Then the mixture was coated onto a copper foil. The foils were dried at 80°C for 4 h and later dried in vacuum at 120°C for 12 h. The electrodes were punched to be a disk with a diameter of 10 mm for electrochemical tests.

Half-cell was used for measuring the cathode performance of the activated carbon electrode. The half-cell was assembled with a lithium metal electrode, and an activated carbon electrode, using 2032 coin cell testing. The internal hybrid supercapacitors were assembled with the activated carbon cathode, and $\text{Li}_4\text{Ti}_5\text{O}_{12}$ anode, using 2032 coin cell testing. The mass ratio of activated carbon to $\text{Li}_4\text{Ti}_5\text{O}_{12}$ was controlled between 1.5 and 1.0. And the electrolyte used in all cells was 1 M LiPF₆ in EC/DMC 1:1 by volume. Besides, coin cell 2032 was also employed to assemble the lithium-ion battery LTO/LiFePO₄ and supercapacitor AC|LiPF₆-EC-DMC|AC (YP-17D/YP-17D) with the same electrolyte. Some data of the electrodes were described in the supplementary information.

A LAND battery tester (Wuhan Jinnuo Electronics Co., Ltd) was employed to evaluate the galvanostatic charge/discharge performance of the half cells and hybrid supercapacitors with voltage window specific to the materials. Equivalent series resistance (ESR) for half cells was calculated using the IR drop which is a rapid voltage change at the initial stage of the discharge^{30,39}. Electrical impedance spectroscopy (EIS) was done with an electrochemical workstation Im6eX (ZAHNER, Germany). EIS was conducted using a sinusoidal signal with mean voltage typically set to open circuit potentials with AC-amplitude of 10 mV over a frequency range of 2 MHz to 0.01 Hz. And ZView software was employed to fit the collected EIS data.

- Zaghib, K. *et al.* Safe and fast-charging Li-ion battery with long shelf life for power applications. *J. power sources* **196**, 3949–3954 (2011).
- Conway, B. E. *Electrochemical Capacitors*. (Kluwer Academic, Plenum Publishers, 1999).
- Kötz, R. & Carlen, M. Principles and applications of electrochemical capacitors. *Electrochim. Acta* **45**, 2483–2498 (2000).
- Simon, P. & Gogotsi, Y. Materials for electrochemical capacitors. *Nat. Mater.* **7**, 845–854 (2008).
- Naoi, K. & Simon, P. New materials and new configurations for advanced electrochemical capacitors. *Electrochem. Soc. Interface* **17**, 34–37 (2008).
- Osaka, T., Liu, X. J., Nojima, M. & Momma, T. An electrochemical double layer capacitor using an activated carbon electrode with gel electrolyte binder. *J. Electrochem. Soc.* **146**, 1724–1729 (1999).
- Tanahashi, I., Yoshida, A. & Nishino, A. Properties of the electric double-layer capacitors composed of activated carbon-fiber cloth electrodes and an organic electrolyte. *Denki Kagaku* **56**, 892–897 (1988).
- Naoi, K., Ishimoto, S., Isobe, Y. & Aoyagi, S. High-rate nano-crystalline $\text{Li}_4\text{Ti}_5\text{O}_{12}$ attached on carbon nano-fibers for hybrid supercapacitors. *J. power sources* **195**, 6250–6254 (2010).
- Conway, B. E. Transition from supercapacitor to battery behavior in electrochemical energy-storage. *J. Electrochem. Soc.* **138**, 1539–1548 (1991).
- Liu, K. C. & Anderson, M. A. Porous nickel oxide/nickel films for electrochemical capacitors. *J. Electrochem. Soc.* **143**, 124–130 (1996).
- Toupin, M., Brousse, T. & Belanger, D. Influence of microstructure on the charge storage properties of chemically synthesized manganese dioxide. *Chem. Mater.* **14**, 3946–3952 (2002).
- Chang, J. K. & Tsai, W. T. Material characterization and electrochemical performance of hydrous manganese oxide electrodes for use in electrochemical pseudocapacitors. *J. Electrochem. Soc.* **150**, A1333–A1338 (2003).
- Khomenko, V., Raymundo-Pinero, E. & Beguin, F. Optimisation of an asymmetric manganese oxide/activated carbon capacitor working at 2 V in aqueous medium. *J. power sources* **153**, 183–190 (2006).
- Zhang, Y. *et al.* Progress of electrochemical capacitor electrode materials: A review. *Inter. J. Hydrogen Energy* **34**, 4889–4899 (2009).
- Naoi, K. 'Nanohybrid Capacitor': The Next Generation Electrochemical Capacitors. *Fuel Cells* **10**, 825–833 (2010).
- Cericola, D. & Kötz, R. Hybridization of rechargeable batteries and electrochemical capacitors: Principles and limits. *Electrochim. Acta* **72**, 1–17 (2012).
- Amatucci, G. G., Badway, F., Du Pasquier, A. & Zheng, T. An asymmetric hybrid nonaqueous energy storage cell. *J. Electrochem. Soc.* **148**, A930–A939 (2001).
- He, Y. *et al.* Gassing in $\text{Li}_4\text{Ti}_5\text{O}_{12}$ -based batteries and its remedy. *Sci. Rep.* **2**, 913; doi:10.1038/srep00913 (2012).
- Li, B. *et al.* Facile synthesis of $\text{Li}_4\text{Ti}_5\text{O}_{12}$ /C composite with super rate performance. *Energy Environ. Sci.* **5**, 9595–9602 (2012).
- Pasquier, A. D., Plitz, I., Gural, J., Badway, F. & Amatucci, G. G. Power-ion battery: bridging the gap between Li-ion and supercapacitor chemistries. *J. power sources* **136**, 160–170 (2004).
- Du Pasquier, A., Plitz, I., Menocal, S. & Amatucci, G. A comparative study of Li-ion battery, supercapacitor and nonaqueous asymmetric hybrid devices for automotive applications. *J. power sources* **115**, 171–178 (2003).
- Chen, C. H. *et al.* Studies of Mg-substituted $\text{Li}_{4-x}\text{Mg}_x\text{Ti}_5\text{O}_{12}$ spinel electrodes ($0 < x <= 1$) for lithium batteries. *J. Electrochem. Soc.* **148**, A102–A104 (2001).
- Takai, S. *et al.* Diffusion coefficient measurement of lithium ion in sintered $\text{Li}_{1.33}\text{Ti}_{1.67}\text{O}_4$ by means of neutron radiography. *Solid State Ionics* **123**, 165–172 (1999).
- Choi, H. S., Kim, T., Im, J. H. & Park, C. R. Preparation and electrochemical performance of hyper-networked $\text{Li}_4\text{Ti}_5\text{O}_{12}$ /carbon hybrid nanofiber sheets for a battery-supercapacitor hybrid system. *Nanotechnology* **22**, (2011).
- Come, J. *et al.* A Non-Aqueous Asymmetric Cell with a Ti_2C -Based Two-Dimensional Negative Electrode. *J. Electrochem. Soc.* **159**, A1368–A1373 (2012).
- Karthikeyan, K. *et al.* Unveiling organic-inorganic hybrids as a cathode material for high performance lithium-ion capacitors. *J. Mater. Chem. A* **1**, 707–714 (2013).
- Snook, G. A., Kao, P. & Best, A. S. Conducting-polymer-based supercapacitor devices and electrodes. *J. power sources* **196**, 1–12 (2011).
- Zhu, Y. *et al.* Microwave assisted exfoliation and reduction of graphite oxide for ultracapacitors. *Carbon* **48**, 2118–2122 (2010).
- Zhu, Y. *et al.* Carbon-Based Supercapacitors Produced by Activation of Graphene. *Science* **332**, 1537–1541 (2011).
- Stoller, M. D. *et al.* Activated graphene as a cathode material for Li-ion hybrid supercapacitors. *Phys. Chem. Chem. Phys.* **14**, 3388–3391 (2012).
- Zhang, S. S., Xu, K. & Jow, T. R. EIS study on the formation of solid electrolyte interface in Li-ion battery. *Electrochim. Acta* **51**, 1636–1640 (2006).
- Cheng, L. *et al.* Carbon-coated $\text{Li}_4\text{Ti}_5\text{O}_{12}$ as a high rate electrode material for Li-ion intercalation. *J. Electrochem. Soc.* **154**, A692–A697 (2007).
- Wu, N. L. & Wang, S. Y. Conductivity percolation in carbon-carbon supercapacitor electrodes. *J. power sources* **110**, 233–236 (2002).
- Zhu, N. *et al.* Graphene as a conductive additive to enhance the high-rate capabilities of electrospun $\text{Li}_4\text{Ti}_5\text{O}_{12}$ for lithium-ion batteries. *Electrochim. Acta* **55**, 5813–5818 (2010).
- Service, R. F. Materials science - New 'supercapacitor' promises to pack more electrical punch. *Science* **313**, 902–902 (2006).
- Gogotsi, Y. & Simon, P. True Performance Metrics in Electrochemical Energy Storage. *Science* **334**, 917–918 (2011).
- Zhai, D., Du, H., Li, B., Zhu, Y. & Kang, F. Porous graphitic carbons prepared by combining chemical activation with catalytic graphitization. *Carbon* **49**, 725–729 (2011).
- Shen, K., Huang, Z.-H., Gan, L. & Kang, F. Graphitic Porous Carbons Prepared by a Modified Template Method. *Chem. Lett.* **38**, 90–91 (2009).
- Show, Y. & Imaizumi, K. Decrease in equivalent series resistance of electric double-layer capacitor by addition of carbon nanotube into the activated carbon electrode. *Diamond and Relat. Mater.* **15**, 2086–2089 (2006).

Acknowledgements

The authors would like to thank the financial support from the National Natural Science Foundation of China (Grant Nos. 51232005 and 50972064), and Ministry of Science and Technology (MOST) of China (Grant 2010DFA72760) for collaboration on cutting-edge technology development of electric vehicle.

Author contributions

Z.-H.H. and F.Y.K. conceived the project. Y.L., Z.-H.H. and W.-C.S. designed the experiments. Y.L. carried out the experiments, and H.-Y.S. carried out the TEM experiment. Y.L., Z.-H.H., Y.Y., W.-C.S., Y.-P.Z. and F.Y.K. discussed the results. Y.L., Z.-H.H. and F.Y.K. wrote the initial manuscript which was approved by all the authors.

Additional information

Supplementary information accompanies this paper at <http://www.nature.com/scientificreports>

Competing financial interests: The authors declare no competing financial interests.

How to cite this article: Lei, Y. *et al.* Porous mesocarbon microbeads with graphitic shells: constructing a high-rate, high-capacity cathode for hybrid supercapacitor. *Sci. Rep.* **3**, 2477; DOI:10.1038/srep02477 (2013).



This work is licensed under a Creative Commons Attribution-NonCommercial-NoDerivs 3.0 Unported license. To view a copy of this license, visit <http://creativecommons.org/licenses/by-nc-nd/3.0>